Short Article

Structure

Structure of an Actinobacterial-Type [NiFe]-Hydrogenase Reveals Insight into O_2-Tolerant H_2 Oxidation

Graphical Abstract

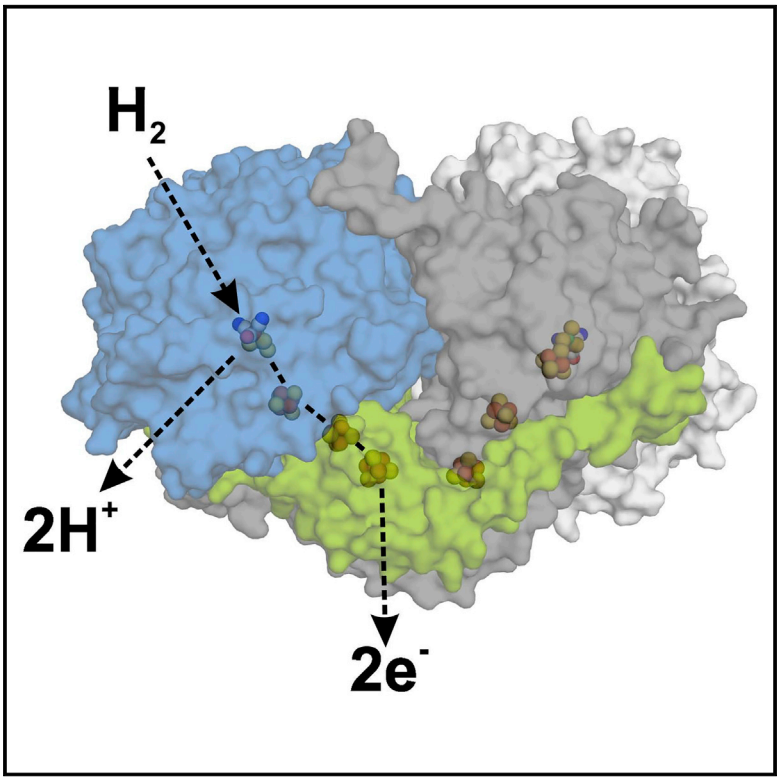

Authors

Caspar Schäfer, Martin Bommer, Sandra E. Hennig, Jae-Hun Jeoung, Holger Dobbek, Oliver Lenz

Correspondence

oliver.lenz@tu-berlin.de (O.L.), holger.dobbek@hu-berlin.de (H.D.)

In Brief

Schäfer et al. report on the first crystal structure of a member of a peculiar group of O_2-tolerant, H_2-converting hydrogenases. Representatives of this novel group have been shown to be able to oxidize even the traces of H_2 present in the atmosphere.

Highlights

- First crystal structure of an actinobacterial-type [NiFe]-hydrogenase
- Stable dimerization is mediated by dedicated peptide extensions
- O_2 tolerance is related to 1 Asp, 3 Cys coordination of [4Fe4S] cluster
- Gas tunnel toward the catalytic center shows atypical architecture

Accession Numbers

5AA5

Schäfer et al., 2016, Structure *24*, 285–292
February 2, 2016
http://dx.doi.org/10.1016/j.str.2015.11.010

CellPress

Structure
Short Article

Structure of an Actinobacterial-Type [NiFe]-Hydrogenase Reveals Insight into O_2-Tolerant H_2 Oxidation

Caspar Schäfer,[1,4] Martin Bommer,[2,4] Sandra E. Hennig,[2] Jae-Hun Jeoung,[2] Holger Dobbek,[2,*] and Oliver Lenz[3,*]
[1]Institut für Biologie/Mikrobiologie, Humboldt-Universität zu Berlin, Chausseestraße 117, 10115 Berlin, Germany
[2]Institut für Biologie/Strukturbiologie, Humboldt-Universität zu Berlin, Philippstraße 13, 10115 Berlin, Germany
[3]Institut für Chemie, Max-Volmer-Laboratorium, Technische Universität Berlin, Straße des 17. Juni 135, 10623 Berlin, Germany
[4]Co-first author
*Correspondence: oliver.lenz@tu-berlin.de (O.L.), holger.dobbek@hu-berlin.de (H.D.)
http://dx.doi.org/10.1016/j.str.2015.11.010
Dedicated to Bärbel Friedrich on the occasion of her 70th birthday on July 29, 2015.

SUMMARY

A novel group of bacterial [NiFe]-hydrogenases is responsible for high-affinity H_2 uptake from the troposphere, and is therefore thought to play an important role in the global H_2 cycle. Here we present the first crystal structure at 2.85-Å resolution of such an actinobacterial-type hydrogenase (AH), which was isolated from the dihydrogen oxidizing bacterium, *Ralstonia eutropha*. The enzyme has a dimeric structure carrying two active [NiFe] sites that are interconnected by six [4Fe4S] clusters over a range of approximately 90 Å. Unlike most other [NiFe]-hydrogenases, the [4Fe4S] cluster proximal to the [NiFe] site is coordinated by three cysteines and one aspartate. Mutagenesis experiments revealed that this aspartate residue is related to the apparent O_2 insensitivity of the AH. Our data provide first structural insight into specialized hydrogenases that are supposed to consume atmospheric H_2 under challenging conditions, i.e. at high O_2 concentration and wide temperature and pH ranges.

INTRODUCTION

The steady-state concentration of molecular hydrogen (H_2) in the atmosphere amounts to 0.5 ppmv (Constant et al., 2009). This value is the outcome of the global H_2 cycle, in which stratospheric photochemistry and mostly anthropogenic processes, including fossil fuel combustion and biomass burning, are the main sources of H_2 (Novelli et al., 1999). Remarkably, more than 80% of the annual turnover, corresponding to ca. 90 Tg a^{-1}, is due to H_2 uptake in soils (Rhee et al., 2006). The major contribution of soil to H_2 uptake was already recognized in the 1990s (Conrad, 1996), but the underlying (bio-) chemical processes remained elusive. Although it has already been speculated that nature's most abundant H_2-cycling biocatalysts, hydrogenases, might be responsible for H_2 uptake in soils, their typically moderate affinity for H_2, with threshold levels for catalytic H_2 turnover 10–100 times higher than the atmospheric H_2 concentration, made this unlikely (Conrad et al., 1983).

It was not until 2008 that the first microorganism able to consume atmospheric H_2 was identified (Constant et al., 2008). This organism, *Streptomyces* sp. PCB7, contains a novel type of hydrogenase, which seems to be abundant in the soil-colonizing actinobacteria (Constant et al., 2011b). Indeed, high-affinity H_2 uptake has been experimentally proven for, e.g., spores of *Streptomyces* sp. PCB7 as well as for starving cultures of the model actinomycete *Mycobacterium smegmatis* and the acidobacterium *Pyrinomonas methylaliphatogenes*. These observations led to the hypothesis that H_2-driven energy conservation may contribute to the survival of these soil-living organisms under challenging conditions (Berney and Cook, 2010; Constant et al., 2011a; Berney et al., 2014; Greening et al., 2015b). Consequently, the high-affinity hydrogenases are suggested to be the key players in hydrogen uptake in the global hydrogen cycle (Constant et al., 2010; Greening et al., 2015c).

This novel type of [NiFe]-hydrogenases was originally classified as group 5 [NiFe]-hydrogenases (Constant et al., 2011b) and was recently re-classified into group 1h (Greening et al., 2015a). While widespread in actinobacterial species, it has been found also in other bacterial lineages. The β-proteobacterium *Ralstonia eutropha*, a strictly respiratory, H_2-oxidizing facultative autotroph containing four catalytically active [NiFe]-hydrogenases (Lenz et al., 2015), represents a prominent example. The actinobacterial-type [NiFe]-hydrogenase (AH) of *R. eutropha* is in fact the first hydrogenase of this type characterized biochemically in its purified form (Schäfer et al., 2013; Greening et al., 2015c). The enzyme consists of two subunits, HofK and HofG, and shows a very low H_2 turnover rate of approximately 0.5 s^{-1}. Its remarkable temperature and pH tolerance is in line with its presumed function under environmentally challenging conditions. Surprisingly, the Michaelis constant for H_2 of the purified enzyme was not sufficiently low to allow efficient oxidation of atmospheric dihydrogen (Schäfer et al., 2013; Greening et al., 2015c). This is in marked contrast to the results for *Streptomyces* sp. PCB7 and *Mycobacterium smegmatis*, which, however, have so far been obtained only with whole cells (Constant et al., 2008; Berney et al., 2014) or cell extracts (Greening et al., 2014).

Table 1. Data Collection and Refinement Statistics

	2.85 Å Data[a]	Extended 2.5 Å Data[b]
Data Collection		
Wavelength (Å)	1.485	1.485
Resolution range (Å)	46.0–2.85 (2.95–2.85)	46.0–2.50 (2.59–2.50)
Space group	$P\,2_1$	$P\,2_1$
Unit cell	81.8, 268.0, 144.7, 90, 106.6, 90	81.8, 268.0, 144.7, 90, 106.6, 90
Total reflections	580,059 (58,197)	788,905 (42,250)
Unique reflections	138,302 (13,820)	200,461 (16,502)
Multiplicity	4.2 (4.2)	3.9 (2.6)
Completeness (%)	99.84 (100.00)	97.36 (80.47)
Mean I/σ (I)	9.95 (2.06)	7.17 (0.55)
Wilson B factor	45.59	33.63
R_{merge}	0.135 (0.716)	0.175 (1.758)
R_{meas}[c]	0.155 (0.820)	0.202 (2.243)
R_{pim}[d]	0.075 (0.397)	0.100 (1.360)
$CC_{1/2}$[e]	0.991 (0.685)	0.987 (0.178)
Refinement		
R_{work}	0.1636 (0.2518)[f]	0.1883 (0.3439)
R_{free}	0.2167 (0.3107)[f]	0.2413 (0.3775)
No. of non-H atoms		42,865
Macromolecules		42,631
Ligands		234
Water		–
Protein residues		5,432
RMSD (bonds)		0.004
RMSD (angles)		0.89
Ramachandran favored (%)		94
Ramachandran outliers (%)		0.35
Clashscore		20.65
Average B factor		46.1
Macromolecules		46.2
Ligands		33.1

Values in parentheses refer to the highest-resolution shell. RMSD, root-mean-square deviation.

[a]Criterion for resolution cut-off: mean I/σ (I) > 2.

[b]Dataset containing additional data resolution shells used in refinement (Karplus and Diederichs, 2012).

[c]Redundancy-independent merging R factor (Diederichs and Karplus, 1997).

[d]Precision-indicating merging R factor (Weiss, 2001).

[e]Pearson correlation coefficient of half datasets (Karplus and Diederichs, 2012).

[f]Calculated from the 2.5-Å refined model using phenix.model_vs_data (Afonine et al., 2010).

In common with all *R. eutropha* hydrogenases, the AH sustains catalytic activity in the presence of ambient O_2 (Schäfer et al., 2013; Lenz et al., 2015). In fact, molecular oxygen apparently does not affect the H_2 conversion activity the AH at all (Schäfer et al., 2013). While ancestral [NiFe]-hydrogenases are O_2 sensitive, more recent lineages of these enzymes have evolved O_2 tolerance/insensitivity, a feature appealing for biotechnological applications (Vincent et al., 2006; Krassen et al., 2011; Lauterbach et al., 2013). Therefore, the understanding of the molecular details of O_2 tolerance has been the focus of hydrogenase research in the past few years, and considerable progress has been made especially in the case of O_2-tolerant membrane-bound [NiFe] hydrogenases (Goris et al., 2011; Evans et al., 2013). In contrast, little is known about the mechanism that makes a hydrogenase virtually insensitive to O_2.

Here, we present the first crystal structure of an apparently O_2-insensitive, actinobacterial-type [NiFe]-hydrogenase, using AH from *R. eutropha* as the model. The structure revealed a tight physical and electronic interaction of two hydrogenase modules and an unusual coordination of the electron-transferring [4Fe4S] cluster proximal to the catalytic center by three cysteine residues and one aspartate. AH variants with alternative cluster coordination lost their apparent O_2 insensitivity.

RESULTS

AH was purified as described previously (Schäfer et al., 2013) from *R. eutropha* cells harboring a plasmid for overexpression of the AH structural genes, *hofKG* (see Experimental Procedures). All genes required for AH biosynthesis, including the specific endopeptidase, were expressed at wild-type level from the endogenous megaplasmid, pHG1, of *R. eutropha* (Schäfer et al., 2013). The purified enzyme was crystallized under an anoxic, reducing atmosphere containing 5% H_2 and formed needle-shaped, brown crystals. The structure of AH was solved by molecular replacement at 2.85 Å (reported) resolution in the space group $P2_1$. Additional data up to 2.5 Å resolution from the same dataset were included to aid refinement (see Table 1 and Experimental Procedures). The basic AH monomer (Figure 1A) displays the typical hydrogenase subunit composition comprising a large subunit, HofG, and a small subunit, HofK. Two AH monomers form a stable $(HofKG)_2$ dimer (Figure 1B), consistent with previous size-exclusion chromatography results (Schäfer et al., 2013).

Residues 19–579 (of 579) and 6–350 (of 351) of HofG and HofK, respectively, could be discerned in the electron density. The residues 305–351 of HofK form a C-terminal extension (Figure 1A) unique to AH-like enzymes. This extension forms a helix structure that mediates physical contact to the second HofK molecule of the dimer. The helices from both HofK subunits are located next to each other and form a large interface for stable dimer interaction (Figure 1B). An additional 12-residue structure present at the N terminus of each HofK subunit directly interacts with the HofG subunit of the other HofKG dimer. In total, the interfacial area of the two HofKG monomers, as calculated by the PISA server (Krissinel and Henrick, 2007), amounts to 5,356 $Å^2$, corresponding to 15.5% of the total surface of a monomer.

Each functional AH module contains a [NiFe] active site in the large subunit and an electron transport relay composed of three [FeS] clusters in the small subunit (Figure 2). Electron density observed at the [NiFe] cluster agrees with the active-site model derived from high-resolution structural data obtained with other [NiFe]-hydrogenases (Figure 2B; Volbeda et al., 1996; Fritsch

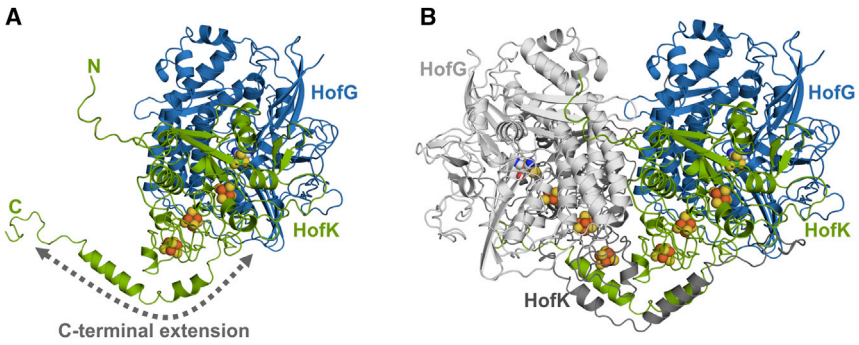

Figure 1. Subunit and Cofactor Composition of the AH from *R. eutropha*

(A) AH monomer (cartoon representation) consisting of the large HofG subunit (blue), which contains the [NiFe] active site and the small HofK subunit (green), which harbors three [4Fe4S] clusters.

(B) Corresponding overall structure composed of two AH monomers (the second monomer is shown in gray colors). (Organo-)metallic cofactors are shown as spheres.

et al., 2011; Ogata et al., 2015). The active-site nickel and iron ions are coordinated by four cysteine-derived thiolates. The iron is further coordinated by one CO and two CN ligands. This architecture is common to all known [NiFe]-hydrogenases (Lubitz et al., 2014). Also, the second coordination sphere of the active site shows no striking compositional or geometric deviations when compared with [NiFe]-hydrogenase from other groups (Figure S1A). One remarkable feature of AH-like enzymes is that the terminal histidine residue, His579, of the large subunit is not involved in coordination of an additional metal ion (magnesium or iron). Such metal coordination is established by an amino acid motif conserved in all other [NiFe]-hydrogenase crystal structures. In actinobacterial-type enzyme, this motif is replaced by another conserved pattern involving a tyrosine residue (Figure S1B).

Residues $Ile83_{HofG}$ and $Leu131_{HofG}$ form a gate between the proposed surface-accessible gas tunnel and the catalytic center (Figure 2B). These amino acid residues have stood in the focus of several studies on the O_2 tolerance/sensitivity of [NiFe]-hydrogenases (Volbeda et al., 2002; Buhrke et al., 2005; Duché et al., 2005; Liebgott et al., 2010). In the case of H_2-sensing, regulatory [NiFe]-hydrogenases, bulky amino acid side chains have been suggested to protect the active site from reacting with O_2 (Buhrke et al., 2005; Duché et al., 2005). The AH gas tunnel gate appears to be quite open, but the average diameter of the tunnel itself is particularly small. Moreover, its spatial position is clearly different from that of other [NiFe]-hydrogenases (Figure S2, Montet et al., 1997; Volbeda et al., 2002; Fritsch et al., 2011). The narrow diameter in particular may result in restricted access of O_2 (and presumably also H_2) to the active site.

The electron transport pathway in the small subunit is composed of three [4Fe4S] clusters (Figure 2A). The [4Fe4S] cluster distal to the active site is coordinated by three cysteines and one histidine, as observed in most other [NiFe]-hydrogenases (Lubitz et al., 2014). The medial [4Fe4S] cluster is coordinated by four cysteines. The proximal [4Fe4S] cluster has a standard cubane-type structure, but displays an unusual coordination with three cysteines and one aspartate ($Asp35_{HofK}$, Figure 2C). $Asp35_{HofK}$ coordinates one Fe ion in the proximal [4Fe4S] cluster as a monodentate ligand. However, a bidentate coordination also appears possible by slightly shifting the carboxylate (Figure 2C). Remarkably, the electron transfer chains of the two monomers are electronically interconnected in the AH dimer. The two distal clusters are separated by only 11.3 Å (Figure 2A), enabling rapid electron transfer between both branches of the electron transfer chain (Page et al., 1999).

The rather unusual coordination of the proximal [4Fe4S] cluster prompted us to investigate the precise role of $Asp35_{HofK}$. We generated variants in which $Asp35_{HofK}$ was replaced by either of Cys, Ser, Asn, Ala, and His, henceforth denoted AH^{D35X}, where X stands for either of C, S, N, A, or H. Surprisingly, most of the variants could be purified in wild-type like amounts, except for AH^{D35H}, which was obtained at low yield and purity (Figure S3). Correspondingly, only low H_2-oxidation activity was measured for this variant (Table 2). These observations suggest that the Asp-to-His exchange impeded the overall structural integrity of the enzyme. In all other cases, active enzyme was synthesized at wild-type level regardless of the altered coordination and/or configuration of the proximal [FeS] cluster.

To investigate systematically the effect of the substitutions on AH activity, we measured the H_2-driven reduction of the artificial electron acceptor nitroblue tetrazolium (NBT) with an inverted Clark electrode in both the absence and presence of O_2. This allowed the quantification of H_2 consumption irrespective of O_2-mediated re-oxidation of NBT. Considerable activities were observed for all AH variants (except AH^{D35H}) when O_2 was absent (Table 2). The activity of AH^{D35N} appeared to be even slightly increased compared with the native protein, while that of AH^{D35S} was reduced. The maximal H_2 oxidation activities measured for all four active AH variants in the presence of 780 μM of O_2 were significantly lower than those obtained upon anaerobic measurement. This is in marked contrast to AH^{WT}, which showed no activity decrease under these conditions. The AH variants could be separated into two groups based on their capability to sustain activity over a period of 5 min. While the AH^{D35S} and AH^{D35C} proteins still showed residual activity 5 min after having reached maximal activity (Table 2), the AH^{D35N} and AH^{D35A} variants apparently lost activity entirely, which was consistent with their inability to consume all of the H_2 in the activity assay (Table 2; Figure 3). In summary, any substitution of $Asp35_{HofK}$ leads to an O_2 sensitivity of the AH catalytic activity, with the D35N and D35A exchanges having the strongest effects.

DISCUSSION

The AH from *R. eutropha* was the first biochemically characterized enzyme of the novel actinobacterial-type [NiFe]-hydrogenases, which are supposed to be the major contributors to H_2 removal from the atmosphere. Among a number of interesting biochemical properties, the apparent O_2 insensitivity of the

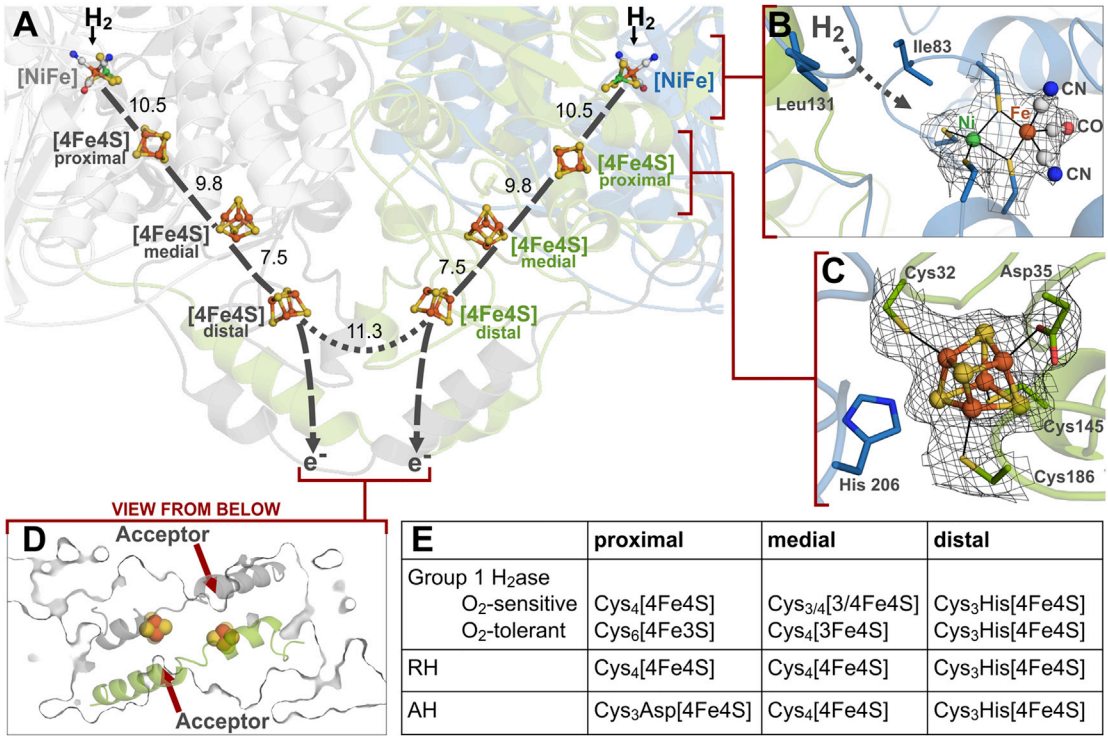

E	proximal	medial	distal
Group 1 H_2ase			
O_2-sensitive	Cys_4[4Fe4S]	$Cys_{3/4}$[3/4Fe4S]	Cys_3His[4Fe4S]
O_2-tolerant	Cys_6[4Fe3S]	Cys_4[3Fe4S]	Cys_3His[4Fe4S]
RH	Cys_4[4Fe4S]	Cys_4[4Fe4S]	Cys_3His[4Fe4S]
AH	Cys_3Asp[4Fe4S]	Cys_4[4Fe4S]	Cys_3His[4Fe4S]

Figure 2. Cofactor Arrangement in the AH

(A) V-Shaped electron transfer chain in the dimeric AH with each of two branches consisting of the [NiFe] active site and three [4Fe4S] clusters. Cofactors are shown as ball-and-stick representation, and the text color indicates the subunit affiliation of each cluster (blue/light gray: HofG subunits; green/dark gray: HofK subunits). Shortest distances between the cofactors are given in ångstroms.

(B) [NiFe] active site of the AH (see Figure S1 for details). Ile83 and Leu131 are the "gate"-forming residues of the proposed gas tunnel (see also Figure S2), which is indicated by the dashed arrow.

(C) Architecture and coordination of the proximal [4Fe4S] cluster of the AH. The gray meshes in (B) and (C) indicate the $2F_o$-F_c electron density at 1.0σ.

(D) Proposed acceptor binding sites of the AH (view from below). The gray outline represents a slice through the surface of the AH, and the helices show the C-terminal extensions of both HofK subunits. The red arrows indicate the site where an acceptor can access in electron transfer distance to the distal [4Fe4S] cluster (shown as spheres).

(E) Table showing a comparison of the typical [FeS]-cluster configurations in different [NiFe]-hydrogenase types (RH, regulatory [NiFe] hydrogenase; see Table S1 for the corresponding redox potentials).

enzyme is outstanding. The crystal structure of the native AH in combination with biochemical data on AH variants lay the foundation for elucidating the molecular basis of these properties.

Over the past few years, molecular mechanisms of O_2 tolerance have been the focus of hydrogenase research, and a detailed mechanism has recently been established for a few O_2-tolerant [NiFe]-hydrogenases. O_2-tolerant MBHs, for instance, were found to contain a unique [4Fe3S] cluster in the position proximal to the [NiFe] active site, and this cofactor was revealed to be crucial for sustained H_2 cycling in the presence of O_2 tolerance of these enzymes (Fritsch et al., 2013). However, as the AH enzyme does not contain a [4Fe3S] cluster, its apparent O_2 insensitivity must rely on other features.

Here we present the first crystal structure of an O_2-tolerant hydrogenase that does not belong to group 1d of membrane-bound [NiFe]-hydrogenases (Greening et al., 2015a), and, indeed, the structural basis for O_2 tolerance seems to be different in the two groups. Our results indicate that the coordination of the proximal [4Fe4S] cluster by $Asp35_{HofK}$, which is conserved in all actinobacterial-type (group 1h) hydrogenases (Figure S4), plays a key role in the apparent O_2 insensitivity of the AH. The contribution of an aspartate to the ligation of a [4Fe4S] cluster is a rare feature and has been reported only for a small number of redox proteins (George et al., 1989; Calzolai et al., 1995; Muraki et al., 2010; Gruner et al., 2011), including F_{420}-reducing [NiFe]-hydrogenase (Vitt et al., 2014). In contrast to AH, the latter enzyme is synthesized exclusively under strictly anaerobic conditions, and the role of its unusual cluster coordination remains elusive. In comparison with an all-cysteine ligation, the involvement of an aspartate in [4Fe4S] cluster coordination is supposed to lead to a moderate increase in the redox potential. In the case of a *Pyrococcus furiosus* ferredoxin, the replacement of an aspartate by a cysteine resulted in an all-Cys ligation and revealed a decrease of the redox potential of the corresponding [4Fe4S] cluster by approximately 60 mV (Brereton et al., 1998). This relies most probably on the electron-withdrawing properties of the aspartate, which stabilizes a reduced state of the cluster. Thus, the aspartate might be engaged by nature to fine-tune the redox potential of the proximal [4Fe4S] cluster in AH. While the selective increase in potential afforded by the aspartate ligand seems beneficial, a further increase, imposed by, e.g., a [3Fe4S] cluster, may be detrimental

Table 2. Specific Activities of the AH^{D35X} Variants in Presence and Absence of O_2

	H_2 Oxidation Activity (U/mg of Protein)[a]		
		With O_2[b]	
Protein	Without O_2	Max.	5 min
AH^{WT}	0.22 ± 0.08	0.22 ± 0.05	0.15 ± 0.04
AH^{D35C}	0.16 ± 0.02	0.08 ± 0.04	0.04 ± 0.03
AH^{D35S}	0.13 ± 0.04	0.07 ± 0.03	0.03 ± 0.02
AH^{D35N}	0.44 ± 0.14	0.30 ± 0.13	0.00 ± 0.05
AH^{D35A}	0.18 ± 0.05	0.09 ± 0.02	0.00 ± 0.04
AH^{D35H}	0.07 ± 0.01	ND	ND

[a]H_2-mediated NBT reduction was measured amperometrically with an inverted Clark-type electrode. Displayed are the mean and SD of measurements done in at least triplicate. ND, not determined.

[b]The assay contained 780 μM O_2. Values represent maximal activities (max.) and activities measured 5 min later. Maximal activity of the AH^{WT} enzyme was observed after a short lag phase of 1–3 min, while for the AH variants, maximal activity was observed immediately (Figure 3). All values reported were determined at H_2 concentrations >20 K_M^{H2} of AH^{wt} (3.6 μM; Schäfer et al., 2013).

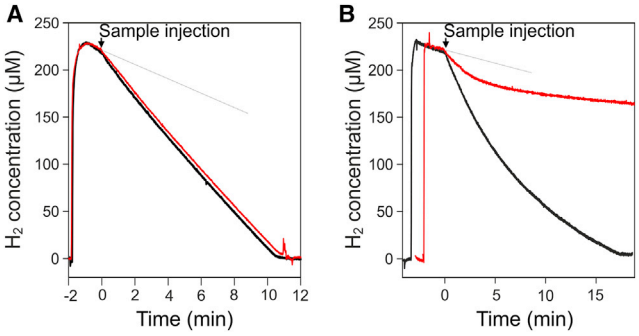

Figure 3. Hydrogen Consumption by Native AH and the AH^{D35N} Variant in the Absence and Presence of O_2

Hydrogen consumption by native AH (A) and the AH^{D35N} variant (B) in the absence (black lines) and presence (red lines) of O_2. H_2-mediated NBT reduction was followed in an amperometric assay under anaerobic conditions or in the presence of 780 μM O_2 (70% saturation). Thin gray lines indicate the enzyme-independent loss of H_2. The subunit pattern of all purified AH variants is shown in Figure S3. The conservation of the cluster-coordinating Asp residue among group 1h [NiFe]-hydrogenases is shown in Figure S4.

for the performance of AH. This is in fact supported by the AH^{D35N} and AH^{D35A} variants showing the most drastic effect on H_2 oxidation activity in the presence of O_2 as they rapidly lost activity. In contrast, the AH^{D35C} and AH^{D35S} proteins retained residual activity while the native AH was not affected at all by O_2. This can be explained by the ability of Cys and Ser to serve as cluster ligands, whereas Asn and Ala do not have such capacity. Because of the missing fourth coordination site, the AH^{D35N} and AH^{D35A} variants contain presumably a [3Fe4S] cluster. [3Fe4S] clusters usually have significantly higher redox potentials than [4Fe4S] clusters (Roberts and Lindahl, 1994; Pershad et al., 1999; Roessler et al., 2012), and conversion of [3Fe4S] clusters into [4Fe4S] clusters by genetic engineering has been shown to lead to significantly lowered redox potentials in fumarate reductase (Manodori et al., 1992) and hydrogenase (Rousset et al., 1998).

Although our 2.85-Å resolution structure of the reduced state of the AH suggests a predominantly monodentate coordination by Asp35, a bidentate coordination cannot be excluded. It has been proposed that *P. furiosus* ferredoxin is able to dynamically alter its cluster potential by switching between such coordination states (Sham et al., 2002).

Our findings suggest that the apparent O_2 insensitivity of AH is not based on bare hindrance of O_2 access to the active site. It rather relies on the fine-tuning of the redox properties of the metal cofactors, supporting a catalytic mechanism for O_2 tolerance. Although the AH gas tunnel obviously does not prevent access of O_2, it may restrict its access rate, and therefore may play a role in the apparent O_2 insensitivity. For O_2-tolerant [NiFe]-hydrogenases from *R. eutropha* (Lauterbach and Lenz, 2013) and *Escherichia coli* (Wulff et al., 2014), it was shown that O_2 is reductively detoxified through fast reverse electron transport, with concomitant release of H_2O and H_2O_2. Though direct evidence has so far not been collected, a similar mechanism might be working in the AH.

The stable dimeric form of the AH provides an additional crucial factor for its remarkable biochemical properties. In the case of membrane-bound [NiFe]-hydrogenases belonging to groups 1a–e (Greening et al., 2015a), dimerization is mediated solely by the globular parts of the two subunits revealing a contact surface of roughly 2,600–2,800 $Å^2$ (calculated from PDB: 3UQY and 4GD3; Ogata et al., 2010; Volbeda et al., 2012, 2013). The contact surface of the group 1h enzyme AH, however, amounts to 5,400 $Å^2$, and thus is approximately twice as large as that of enzymes in groups 1a–e. The enlarged interface between the two monomers may contribute to the previously reported high temperature and pH stability of the AH (Schäfer et al., 2013).

The C-terminal extension of the AH small subunit, and to a lesser extent the N-terminal extension, are considerably involved in the enlargement of the contact surface. C-Terminal extensions are also found in small subunits of membrane-bound and regulatory [NiFe]-hydrogenase (RH). In the latter, the extension also enables dimer formation, and additionally mediates the contact to the cognate histidine protein kinase, which is absolutely required for the H_2 sensory function (Buhrke et al., 2004). In the case of membrane-bound [NiFe]-hydrogenases, the C-terminal extension anchors the protein in the cytoplasmic membrane and provides a connection to the physiological redox partner, a *b*-type cytochrome (Volbeda et al., 2013). The C-terminal extensions of the AH dimer may provide an amphipathic contact site to the cytoplasmic membrane. According to the crystal structure, however, they seem to shield the two distal [4Fe4S] clusters in the dimer, which, compared to other [NiFe]-hydrogenases, are buried below the protein surface with an Fe edge-to-surface distance of at least 12 Å. The immediate physiological electron acceptor may have access only through a small cavity with only 6-Å distance to the distal cluster (Figures 2A and 2D). The physiological electron acceptor of actinobacterial-like hydrogenases is still unknown, although the enzymes are thought to be coupled to the aerobic respiratory chain (Schäfer et al., 2013; Greening et al., 2014).

In the AH dimer, the distal [4Fe4S] clusters are located within distance of physiological electron transfer (Page et al., 1999), suggesting that the electron transport chains of the two

functional units are electronically interconnected. A similar arrangement has been previously observed for the membrane-associated group 1 [NiFe]-hydrogenase from *Allochromatium vinosum* (Ogata et al., 2010) and *E. coli* (Volbeda et al., 2012). The AH carries a [4Fe4S] cluster in the medial position (most group 1 enzymes possess a [3Fe4S] cluster in the corresponding position; Figure 2E and Table S1), which may facilitate electron transfer between the two functional units without high thermodynamic barriers. In the case of O_2 attack, electrons derived from a still functional module of an AH dimer could be easily transferred to the second monomer and contribute to reductive reactivation of an O_2-inactivated [NiFe] active site, as proposed for O_2-tolerant membrane-bound hydrogenase from *E. coli* (Volbeda et al., 2013). In fact, it has been shown for the *E. coli* enzyme that an oxidatively inactivated monomer can be brought back to work with electrons provided by reverse electron flow from another monomer (Wait et al., 2010). Whether a combined mechanism of restricted access and reductive removal of O_2 is instrumental in actinobacterial-type [NiFe]-hydrogenases awaits further studies.

The structure of the *R. eutropha* AH provides a first insight into the configuration of an important class of enzymes directly involved in the tropospheric H_2 cycle. The tight packing of the AH dimer, and the dedicated metal cofactor arrangement and coordination, contribute to the stability and apparent O_2 sensitivity of the enzyme, to which the size and unprecedented position of the putative gas tunnel might contribute substantially. Further biochemical, electrochemical, and spectroscopic studies are needed to provide a rationale for the low catalytic H_2 turnover and unusually high affinity for H_2, which are hallmarks of most actinobacterial-type hydrogenases.

EXPERIMENTAL PROCEDURES

Enzyme Purification and Crystallization

For homologous overproduction of the AH variants in *R. eutropha*, suitable overexpression plasmids were constructed (see Supplemental Experimental Procedures for details). Growth of the recombinant strains and subsequent purification of the AH variants by *Strep*-Tactin affinity chromatography was done as previously described (Schäfer et al., 2013). Crystallization conditions were screened with purified native AH under anoxic conditions (95% N_2, 5% H_2) using the sitting-drop method. First, commercially available screens were tested, in which crystals grew at 19°C within a period of 24 hr to several weeks. Optimized crystals suitable for X-ray diffraction analysis grew in 17.5% polyethylene glycol 4000 and 160 mM imidazole-malonate (pH 7.0), and were frozen in liquid N_2 with 15% (2*R*,3*R*)-2,3-butanediol as cryo-protectant.

Data Collection and Structure Determination

Diffraction data were collected from a single crystal on BL14.1 operated by the Helmholtz-Zentrum Berlin (HZB) at the BESSY II electron storage ring (Berlin-Adlershof; Mueller et al., 2012). Data were integrated with XDS (Kabsch, 2010) and XDSAPP (Krug et al., 2012). Two sets of data collection and refinement statistics are presented in Table 1. The 2.85-Å dataset corresponds to the data truncated using the $I/\sigma(I) > 2$ convention, and this is the resolution reported here. The 2.5-Å dataset contains additional resolution shells used in refinement (Karplus and Diederichs, 2012). The structure was solved by molecular replacement using Phaser (McCoy et al., 2007), using the structure of *Desulfomicrobium baculatum* [NiFeSe] hydrogenase (PDB: 1CC1) as search model. The structure was built in Coot (Emsley et al., 2010), refined with phenix.refine (Afonine et al., 2012), and validated with MolProbity (Chen et al., 2010). The asymmetric unit contained six AH monomers arranged as three independent $(HofKG)_2$ dimers. In the absence of contrary evidence, the geometry of the [NiFe] cluster was restrained to that of the 1.5-Å structure of H_2-reduced *R. eutropha* MBH (PDB: 3RGW; Fritsch et al., 2011) using eLBOW (Moriarty et al., 2009). Interaction surfaces were calculated by the PISA server (Krissinel and Henrick, 2007), and the structure was visualized using PyMOL (Schrödinger).

Biochemical Assays

H_2 uptake activities were followed spectrophotometrically using the artificial electron acceptor NBT. The O_2 tolerance was measured amperometrically with a modified Clark electrode. Both assays were described previously (Schäfer et al., 2013).

ACCESSION NUMBERS

The atomic coordinates and structure factors have been deposited in the PDB, www.pdb.org, under the PDB: 5AA5.

SUPPLEMENTAL INFORMATION

Supplemental Information includes Supplemental Experimental Procedures, four figures, and two tables and can be found with this article online at http://dx.doi.org/10.1016/j.str.2015.11.010.

AUTHOR CONTRIBUTIONS

C.S., S.H., H.D., and O.L. designed research; C.S, M.B., and S.H. performed research; C.S., M.B., S.H., J.-H.J., H.D., and O.L. analyzed data; and C.S., M.B., H.D., and O.L. wrote the paper.

ACKNOWLEDGMENTS

The work of C.S. was funded by the German Ministry of Science and Education (BMBF project "H_2 Design Cell"). We acknowledge access to beamlines of the BESSY II storage ring (Berlin, Germany) via the Joint Berlin MX-Laboratory sponsored by the Helmholtz Zentrum Berlin für Materialien und Energie, the Freie Universität Berlin, the Humboldt-Universität zu Berlin, the Max-Delbrück-Centrum and the Leibniz-Institut für Molekulare Pharmakologie. H.D. and O.L. acknowledge support by the Cluster of Excellence "Unifying Concepts in Catalysis (UniCat)."

Received: October 5, 2015
Revised: November 19, 2015
Accepted: November 20, 2015
Published: December 31, 2015

REFERENCES

Afonine, P.V., Grosse-Kunstleve, R.W., Chen, V.B., Headd, J.J., Moriarty, N.W., Richardson, J.S., Richardson, D.C., Urzhumtsev, A., Zwart, P.H., and Adams, P.D. (2010). phenix.model_vs_data: a high-level tool for the calculation of crystallographic model and data statistics. J. Appl. Crystallogr. *43*, 669–676.

Afonine, P.V., Grosse-Kunstleve, R.W., Echols, N., Headd, J.J., Moriarty, N.W., Mustyakimov, M., Terwilliger, T.C., Urzhumtsev, A., Zwart, P.H., and Adams, P.D. (2012). Towards automated crystallographic structure refinement with phenix.refine. Acta. Crystallogr. D Biol. Crystallogr. *68*, 352–367.

Berney, M., and Cook, G.M. (2010). Unique flexibility in energy metabolism allows mycobacteria to combat starvation and hypoxia. PLoS One *5*, e8614.

Berney, M., Greening, C., Hards, K., Collins, D., and Cook, G.M. (2014). Three different [NiFe]-hydrogenases confer metabolic flexibility in the obligate aerobe *Mycobacterium smegmatis*. Environ. Microbiol. *16*, 318–330.

Brereton, P.S., Verhagen, M.F., Zhou, Z.H., and Adams, M.W. (1998). Effect of iron-sulfur cluster environment in modulating the thermodynamic properties and biological function of ferredoxin from *Pyrococcus furiosus*. Biochemistry *37*, 7351–7362.

Buhrke, T., Lenz, O., Porthun, A., and Friedrich, B. (2004). The H_2-sensing complex of *Ralstonia eutropha*: interaction between a regulatory [NiFe] hydrogenase and a histidine protein kinase. Mol. Microbiol. *51*, 1677–1689.

Buhrke, T., Lenz, O., Krauss, N., and Friedrich, B. (2005). Oxygen tolerance of the H_2-sensing [NiFe] hydrogenase from *Ralstonia eutropha* H16 is based on limited access of oxygen to the active site. J. Biol. Chem. *280*, 23791–23796.

Calzolai, L., Gorst, C.M., Zhao, Z.H., Teng, Q., Adams, M.W., and La Mar, G.N. (1995). 1H-NMR investigation of the electronic and molecular structure of the four-iron cluster ferredoxin from the hyperthermophile *Pyrococcus furiosus*. Identification of Asp 14 as a cluster ligand in each of the four redox states. Biochemistry *34*, 11373–11384.

Chen, V.B., Arendall, W.B., Headd, J.J., Keedy, D.A., Immormino, R.M., Kapral, G.J., Murray, L.W., Richardson, J.S., and Richardson, D.C. (2010). MolProbity: all-atom structure validation for macromolecular crystallography. Acta. Crystallogr. D Biol. Crystallogr. *66*, 12–21.

Conrad, R. (1996). Soil microorganisms as controllers of atmospheric trace gases (H_2, CO, CH_4, OCS, N_2O, and NO. Microbiol. Rev. *60*, 609–640.

Conrad, R., Aragno, M., and Seiler, W. (1983). The inability of hydrogen bacteria to utilize atmospheric hydrogen is due to threshold and affinity for hydrogen. FEMS Microbiol. Lett. *18*, 207–210.

Constant, P., Poissant, L., and Villemur, R. (2008). Isolation of *Streptomyces* sp. PCB7, the first microorganism demonstrating high-affinity uptake of tropospheric H_2. ISME J. *2*, 1066–1076.

Constant, P., Poissant, L., and Villemur, R. (2009). Tropospheric H_2 budget and the response of its soil uptake under the changing environment. Sci. Total Environ. *407*, 1809–1823.

Constant, P., Chowdhury, S.P., Pratscher, J., and Conrad, R. (2010). Streptomycetes contributing to atmospheric molecular hydrogen soil uptake are widespread and encode a putative high-affinity [NiFe]-hydrogenase. Environ. Microbiol. *12*, 821–829.

Constant, P., Chowdhury, S.P., Hesse, L., and Conrad, R. (2011a). Co-localization of atmospheric H_2 oxidation activity and high affinity H_2-oxidizing bacteria in non-axenic soil and sterile soil amended with *Streptomyces* sp PCB7. Soil Biol. Biochem. *43*, 1888–1893.

Constant, P., Chowdhury, S.P., Hesse, L., Pratscher, J., and Conrad, R. (2011b). Genome data mining and soil survey for the novel group 5 [NiFe]-hydrogenase to explore the diversity and ecological importance of presumptive high-affinity H_2-oxidizing bacteria. Appl. Environ. Microbiol. *77*, 6027–6035.

Diederichs, K., and Karplus, P.A. (1997). Improved R-factors for diffraction data analysis in macromolecular crystallography. Nat. Struct. Biol. *4*, 269–275.

Duché, O., Elsen, S., Cournac, L., and Colbeau, A. (2005). Enlarging the gas access channel to the active site renders the regulatory hydrogenase HupUV of *Rhodobacter capsulatus* O_2 sensitive without affecting its transductory activity. FEBS J. *272*, 3899–3908.

Emsley, P., Lohkamp, B., Scott, W.G., and Cowtan, K. (2010). Features and development of Coot. Acta. Crystallogr. D Biol. Crystallogr. *66*, 486–501.

Evans, R.M., Parkin, A., Roessler, M.M., Murphy, B.J., Adamson, H., Lukey, M.J., Sargent, F., Volbeda, A., Fontecilla-Camps, J.C., and Armstrong, F.A. (2013). Principles of sustained enzymatic hydrogen oxidation in the presence of oxygen—the crucial influence of high potential Fe-S clusters in the electron relay of [NiFe]-hydrogenases. J. Am. Chem. Soc. *135*, 2694–2707.

Fritsch, J., Scheerer, P., Frielingsdorf, S., Kroschinsky, S., Friedrich, B., Lenz, O., and Spahn, C.M.T. (2011). The crystal structure of an oxygen-tolerant hydrogenase uncovers a novel iron-sulphur centre. Nature *479*, 249–252.

Fritsch, J., Lenz, O., and Friedrich, B. (2013). Structure, function and biosynthesis of O_2-tolerant hydrogenases. Nat. Rev. Microbiol. *11*, 106–114.

George, S.J., Armstrong, F.A., Hatchikian, E.C., and Thomson, A.J. (1989). Electrochemical and spectroscopic characterization of the conversion of the 7Fe into the 8Fe-form of ferredoxin-III from *Desulfovibrio africanus*—Identification of a [4Fe-4S] cluster with one non-cysteine ligand. Biochem. J. *264*, 275–284.

Goris, T., Wait, A.F., Saggu, M., Fritsch, J., Heidary, N., Stein, M., Zebger, I., Lendzian, F., Armstrong, F.A., Friedrich, B., et al. (2011). A unique iron-sulfur cluster is crucial for oxygen tolerance of a [NiFe]-hydrogenase. Nat. Chem. Biol. *7*, 310–318.

Greening, C., Berney, M., Hards, K., Cook, G.M., and Conrad, R. (2014). A soil actinobacterium scavenges atmospheric H_2 using two membrane-associated, oxygen-dependent [NiFe] hydrogenases. Proc. Natl. Acad. Sci. USA *111*, 4257–4261.

Greening, C., Biswas, A., Carere, C.R., Jackson, C.J., Taylor, M.C., Stott, M.B., Cook, G.M., and Morales, S.E. (2015a). Genomic and metagenomic surveys of hydrogenase distribution indicate H_2 is a widely utilised energy source for microbial growth and survival. ISME J. http://dx.doi.org/10.1038/ismej.2015.153.

Greening, C., Carere, C.R., Rushton-Green, R., Harold, L.K., Hards, K., Taylor, M.C., Morales, S.E., Stott, M.B., and Cook, G.M. (2015b). Persistence of the dominant soil phylum acidobacteria by trace gas scavenging. Proc. Natl. Acad. Sci. USA *112*, 10497–10502.

Greening, C., Constant, P., Hards, K., Morales, S., Oakeshott, J.G., Russell, R.J., Taylor, M.C., Berney, M., Conrad, R., and Cook, G.M. (2015c). Atmospheric hydrogen scavenging: from enzymes to ecosystems. Appl. Environ. Microbiol. *81*, 1190–1199.

Gruner, I., Frädrich, C., Böttger, L.H., Trautwein, A.X., Jahn, D., and Härtig, E. (2011). Aspartate 141 is the fourth ligand of the oxygen-sensing $[4Fe\text{-}4S]^{2+}$ cluster of *Bacillus subtilis* transcriptional regulator Fnr. J. Biol. Chem. *286*, 2017–2021.

Kabsch, W. (2010). XDS. Acta. Crystallogr. D Biol. Crystallogr. *66*, 125–132.

Karplus, P.A., and Diederichs, K. (2012). Linking crystallographic model and data quality. Science *336*, 1030–1033.

Krassen, H., Ott, S., and Heberle, J. (2011). In vitro hydrogen production—using energy from the sun. Phys. Chem. Chem. Phys. *13*, 47–57.

Krissinel, E., and Henrick, K. (2007). Inference of macromolecular assemblies from crystalline state. J. Mol. Biol. *372*, 774–797.

Krug, M., Weiss, M.S., Heinemann, U., and Mueller, U. (2012). XDSAPP: a graphical user interface for the convenient processing of diffraction data using XDS. J. Appl. Crystallogr. *45*, 568–572.

Lauterbach, L., and Lenz, O. (2013). Catalytic production of hydrogen peroxide and water by oxygen-tolerant [NiFe]-hydrogenase during H_2 cycling in the presence of O_2. J. Am. Chem. Soc. *135*, 17897–17905.

Lauterbach, L., Lenz, O., and Vincent, K.A. (2013). H_2-driven cofactor regeneration using $NAD(P)^+$-reducing hydrogenases. FEBS J. *280*, 3058–3068.

Lenz, O., Lauterbach, L., Frielingsdorf, S., and Friedrich, B. (2015). Oxygen-tolerant hydrogenases and their biotechnological potential. In Biohydrogen, M. Rögner, ed. (De Gruyter), pp. 61–88.

Liebgott, P.P., Leroux, F., Burlat, B., Dementin, S., Baffert, C., Lautier, T., Fourmond, V., Ceccaldi, P., Cavazza, C., Meynial-Salles, I., et al. (2010). Relating diffusion along the substrate tunnel and oxygen sensitivity in hydrogenase. Nat. Chem. Biol. *6*, 63–70.

Lubitz, W., Ogata, H., Rüdiger, O., and Reijerse, E. (2014). Hydrogenases. Chem. Rev. *114*, 4081–4148.

Manodori, A., Cecchini, G., Schröder, I., Gunsalus, R.P., Werth, M.T., and Johnson, M.K. (1992). [3Fe-4S] to [4Fe-4S] cluster conversion in *Escherichia coli* fumarate reductase by site-directed mutagenesis. Biochemistry *31*, 2703–2712.

McCoy, A.J., Grosse-Kunstleve, R.W., Adams, P.D., Winn, M.D., Storoni, L.C., and Read, R.J. (2007). Phaser crystallographic software. J. Appl. Crystallogr. *40*, 658–674.

Montet, Y., Amara, P., Volbeda, A., Vernede, X., Hatchikian, E.C., Field, M.J., Frey, M., and Fontecilla-Camps, J.C. (1997). Gas access to the active site of Ni-Fe hydrogenases probed by X-ray crystallography and molecular dynamics. Nat. Struct. Biol. *4*, 523–526.

Moriarty, N.W., Grosse-Kunstleve, R.W., and Adams, P.D. (2009). electronic Ligand Builder and Optimization Workbench (eLBOW): a tool for ligand coordinate and restraint generation. Acta. Crystallogr. D Biol. Crystallogr. *65*, 1074–1080.

Mueller, U., Darowski, N., Fuchs, M.R., Förster, R., Hellmig, M., Paithankar, K.S., Puhringer, S., Steffien, M., Zocher, G., and Weiss, M.S. (2012). Facilities for macromolecular crystallography at the Helmholtz-Zentrum Berlin. J. Synchrotron Radiat. *19*, 442–449.

Muraki, N., Nomata, J., Ebata, K., Mizoguchi, T., Shiba, T., Tamiaki, H., Kurisu, G., and Fujita, Y. (2010). X-ray crystal structure of the light-independent protochlorophyllide reductase. Nature *465*, 110–114.

Novelli, P.C., Lang, P.M., Masarie, K.A., Hurst, D.F., Myers, R., and Elkins, J.W. (1999). Molecular hydrogen in the troposphere. Global distribution and budget. J. Geophys. Res. *104*, 30427–30444.

Ogata, H., Kellers, P., and Lubitz, W. (2010). The crystal structure of the [NiFe] hydrogenase from the photosynthetic bacterium *Allochromatium vinosum*: characterization of the oxidized enzyme (Ni-A state). J. Mol. Biol. *402*, 428–444.

Ogata, H., Nishikawa, K., and Lubitz, W. (2015). Hydrogens detected by subatomic resolution protein crystallography in a [NiFe] hydrogenase. Nature *520*, 571–574.

Page, C.C., Moser, C.C., Chen, X., and Dutton, P.L. (1999). Natural engineering principles of electron tunnelling in biological oxidation-reduction. Nature *402*, 47–52.

Pershad, H.R., Duff, J.L., Heering, H.A., Duin, E.C., Albracht, S.P., and Armstrong, F.A. (1999). Catalytic electron transport in *Chromatium vinosum*: application of voltammetry in detecting redox-active centers and establishing that hydrogen oxidation is very fast even at potentials close to the reversible H^+/H_2 value. Biochemistry *38*, 8992–8999.

Rhee, T.S., Brenninkmeijer, C.A.M., and Röckmann, T. (2006). The overwhelming role of soils in the global atmospheric hydrogen cycle. Atmos. Chem. Phys. *6*, 1611–1625.

Roberts, L.M., and Lindahl, P.A. (1994). Analysis of oxidative titrations of *Desulfovibrio gigas* hydrogenase; implications for the catalytic mechanism. Biochemistry *33*, 14339–14350.

Roessler, M.M., Evans, R.M., Davies, R.A., Harmer, J., and Armstrong, F.A. (2012). EPR spectroscopic studies of the Fe-S clusters in the O_2-tolerant [NiFe]-hydrogenase Hyd-1 from *Escherichia coli* and characterization of the unique [4Fe-3S] cluster by HYSCORE. J. Am. Chem. Soc. *134*, 15581–15594.

Rousset, M., Montet, Y., Guigliarelli, B., Forget, N., Asso, M., Bertrand, P., Fontecilla-Camps, J.C., and Hatchikian, E.C. (1998). [3Fe-4S] to [4Fe-4S] cluster conversion in *Desulfovibrio fructosovorans* [NiFe] hydrogenase by site-directed mutagenesis. Proc. Natl. Acad. Sci. USA *95*, 11625–11630.

Schäfer, C., Friedrich, B., and Lenz, O. (2013). Novel, oxygen-insensitive group 5 [NiFe]-hydrogenase in *Ralstonia eutropha*. Appl. Environ. Microbiol. *79*, 5137–5145.

Sham, S., Calzolai, L., Wang, P.L., Bren, K., Haarklau, H., Brereton, P.S., Adams, M.W., and La Mar, G.N. (2002). A solution NMR molecular model for the aspartate-ligated, cubane cluster containing ferredoxin from the hyperthermophilic archeaon *Pyrococcus furiosus*. Biochemistry *41*, 12498–12508.

Vincent, K.A., Cracknell, J.A., Clark, J.R., Ludwig, M., Lenz, O., Friedrich, B., and Armstrong, F.A. (2006). Electricity from low-level H_2 in still air—an ultimate test for an oxygen tolerant hydrogenase. Chem. Comm. (Camb.), 5033–5035.

Vitt, S., Ma, K., Warkentin, E., Moll, J., Pierik, A.J., Shima, S., and Ermler, U. (2014). The F_{420}-reducing [NiFe]-hydrogenase complex from *Methanothermobacter marburgensis*, the first X-ray structure of a group 3 family member. J. Mol. Biol. *426*, 2813–2826.

Volbeda, A., Garcin, E., Piras, C., DeLacey, A.L., Fernandez, V.M., Hatchikian, E.C., Frey, M., and Fontecilla-Camps, J.C. (1996). Structure of the [NiFe] hydrogenase active site: evidence for biologically uncommon Fe ligands. J. Am. Chem. Soc. *118*, 12989–12996.

Volbeda, A., Montet, Y., Vernede, X., Hatchikian, E.C., and Fontecilla-Camps, J.C. (2002). High-resolution crystallographic analysis of *Desulfovibrio fructiosovorans* [NiFe] hydrogenase. Int. J. Hydrogen Energy *27*, 1449–1461.

Volbeda, A., Amara, P., Darnault, C., Mouesca, J.M., Parkin, A., Roessler, M.M., Armstrong, F.A., and Fontecilla-Camps, J.C. (2012). X-ray crystallographic and computational studies of the O_2-tolerant [NiFe]-hydrogenase 1 from *Escherichia coli*. Proc. Natl. Acad. Sci. USA *109*, 5305–5310.

Volbeda, A., Darnault, C., Parkin, A., Sargent, F., Armstrong, F.A., and Fontecilla-Camps, J.C. (2013). Crystal structure of the O_2-tolerant membrane-bound hydrogenase 1 from *Escherichia coli* in complex with its cognate cytochrome *b*. Structure *21*, 184–190.

Wait, A.F., Parkin, A., Morley, G.M., dos Santos, L., and Armstrong, F.A. (2010). Characteristics of enzyme-based hydrogen fuel cells using an oxygen-tolerant hydrogenase as the anodic catalyst. J. Phys. Chem. C *114*, 12003–12009.

Weiss, M.S. (2001). Global indicators of X-ray data quality. J. Appl. Crystallogr. *34*, 130–135.

Wulff, P., Day, C.C., Sargent, F., and Armstrong, F.A. (2014). How oxygen reacts with oxygen-tolerant respiratory [NiFe]-hydrogenases. Proc. Natl. Acad. Sci. USA *111*, 6606–6611.

